Fatigue Life Models for SnAgCu and SnPb Solder Joints Evaluated by Experiments and Simulation

A. Schubert†, R. Dudek, E. Auerswald, A. Gollhardt, B. Michel, H. Reichl
Fraunhofer Institute for Reliability and Microintegration, Berlin,
Gustav-Meyer-Allee 25, D-13355 Berlin, Germany
email: dudek@che.izm.fhg.de

Abstract

In recent years, many solder fatigue models have been developed to predict the fatigue life of solder joints under thermal cycle conditions. While a variety of life prediction models have been proposed for near eutectic SnPb(Ag)-solder joints in the literature, not enough work has been reported in extending these models to lead-free soldered assemblies. The development of life prediction models requires a deep insight into failure modes, constitutive models for the thermo-mechanical behavior of solders and an experimental reliability database. This is needed for the correlation of experimentally determined cycles-to-failure to simulation results by finite-element analysis.

This paper describes in detail the life-prediction models of SnPb(Ag) and SnAgCu solder joints for thermal cycle conditions. To obtain reliable FEM input and to verify simulation results, a variety of material testing and experimental fatigue data is necessary. The accuracy of life-prediction tools has also become critically important, as the designs need to be evaluated and improved with a high degree of reliability, not through relative comparison but by providing absolute numbers.

This work deals with the effect of different solder interconnect alloys (Sn59Pb40Ag1 and Sn95.5Ag3.8Cu0.7) and the effect of different package types (PBGAs, CSPs, Flip Chip on FR-4 with and without underfill) on the fatigue life. Different temperature cycling conditions are applied.

Introduction

Since solder joints provide the mechanical and electrical interconnect between the package and the board, they are susceptible to failures during thermal cycling. For this reason, ensuring the solder joint reliability is one of the most critical design aspects of electronic assemblies. Solder joints of electronic assemblies are complex elements and therefore building accuracy in a life prediction model is not an easy task. The acknowledged complexity arises from the following: The 3-dimensional package structures with solder joints are subjected to multi-axial nonlinear material behaviors, complex joint shapes, and multi-axial loading. In a more specific sense the accuracy of life time predictions depends on the understanding and the consideration of the following problems:

- The solder joints of a component are not all the same: Distances to the neutral point (DNP), height tolerances, and variability in joint geometry and metallurgy vary.
- The initial microstructure can vary (e.g. grain size, intermetallics size and dispersion): Changes in the solder-microstructure can be observed during testing and service conditions, and their influence on the thermo-mechanical properties are not very well understood.
- The effects of substrate finishes and component finishes on the reliability: Soft solders react with metallizations to form interfacial intermetallics. Intermetallics grow with time and temperature. Metallization consumption by intermetallic growth and intermetallics within the solder can be observed.Often the soldering process itself induces anomalies (e.g. changes in the reflow temperature profile, different cooling rates, excessive voids inside the solder, brittle phase formation, concentration gradients of elemental or metallurgical composition when the joint is formed).Smaller solder joints may impose increased interfacial effects and decreased fatigue-creep phenomena (joint volume versus interfacial effects).
- The mechanical behavior of solder is non-linear and temperature dependent. Solder alloys in consideration are above 0.5 of their melting point at –40 °C, so creep processes are expected to dominate the deformation kinetics.
- Failure of solder joints is a complex sequence of possible failure mechanisms involving grain/phase coarsening, grain boundary sliding, matrix creep, micro-void formation and linking, resulting in crack initiation and crack propagation. In the case of SnAgCu solder joints, the damage accumulation process leads to much less coarsening of the microstructure.
- The failure criterion used for recording lifetime might vary, based on either mechanical cracks or electrical failure. Most often, electrical opens resulting from solder joint failures are intermittent and may be difficult to detect accurately (on-line vs. off-line measurements, electrical vs. mechanical damage).

In the past, efforts have been made in characterizing lead-free solders to analyze the temperature and stress dependent inelastic behavior (creep and stress relaxation) and to understand the differences in bulk and joint behavior.

But much work still needs to be done for lead-free solder interconnects in the following areas:

- Failure mechanisms related to the solder joints of the new solder alloys (will creep deformation still play a dominant role for e.g. thermally induced low cycle fatigue?),
- Temperature cycle data, for instance, on real components (acceleration factors may depend on accelerated test conditions and solder alloys) and
- Life prediction models (e.g. a Manson-Coffin type model based on creep strains accumulated in one thermal cycle or an analogous model based on viscoplastic strain energy densities dissipated per cycle).

This paper presents life prediction approaches based on two damage parameters: creep strains accumulated in one thermal cycle and the viscoplastic strain energy density

dissipated per cycle for both SnPb(Ag) and SnAgCu solder joints which are accurate within 2X of actual life measurements.

Constitutive Relations of Solders

All of the alloys studied here are above half of their melting point at use temperatures, so creep processes are expected to dominate the deformation kinetics. The majority of creep models concern the stress- and temperature-dependence of steady-state creep.

Steady-state Creep

Sn59Pb40Ag1-Solder

Grivas et al. [1] suggested that a fine-grained (fine-phased) SnPb(Ag) eutectic alloy exhibited both superplastic deformation and matrix creep deformation. It was assumed that both deformation modes occur simultaneously via independent mechanisms. Superplastic deformation is rate-controlled at "lower" stresses (region II) and matrix creep deformation is rate controlling at "intermediate" stresses (region III). Combining the rates of the two deformation mechanisms, a semi-empirical equation was developed summing up the strain rates in both stress regions, so that

$$\frac{d\varepsilon_S}{dt} = \frac{A_{II}}{T}\sigma^{n_{II}} \exp\left(\frac{-Q_{a,II}}{kT}\right) + \frac{A_{III}}{T}\sigma^{n_{III}} \exp\left(\frac{-Q_{a,III}}{kT}\right), \qquad (1)$$

where $\frac{d\varepsilon_s}{dt}$ is the steady-state strain rate, k is the Boltzmann's constant, T is the absolute temperature, σ is the applied stress, n_{II} and n_{III} are the stress exponents, and A_{II} and A_{III} are constants. Neglecting the dependence of Young's modulus on temperature, the activation energies are apparent ones.

The data given by Grivas et al. [1] and Hacke et al. [2] contains these parameters and these data agree with our experimental creep results measured on Sn59Pb40Ag1 solder (Table 1).

Table 1: Deformation constants of the steady-state creep for Sn59Pb40Ag1, based on own measurements (equation (1))

Region	A ($K s^{-1}$)	n	Q_a (eV)
II	426.95	1.87	0.50
III	94.36	6.74	0.79

Sn95.5Ag3.8Cu0.7-Solder

The alloy composition and microstructure and thus the steady-state creep rate of the examined lead-free solder is dramatically different from the eutectic SnPb(Ag) solder, as was already discussed in [3]. The steady-state creep of SnAgCu solder can be described reasonably well by a hyperbolic sine stress function (Figure 1). At "intermediate" stresses (region III), the strain rate depends on stress to the power, n. At "high" stresses (region IV), the strain rate is an exponential function of stress. This power law break-down region can be described by the simple expression

$$\frac{d\varepsilon_S}{dt} = C_{III,IV}[\sinh(\alpha\sigma)]^n \exp\left(\frac{-Q_a}{kT}\right), \qquad (2)$$

where α prescribes the stress level at which the power law dependence breaks down. Q_a is the apparent activation energy and $C_{III,IV}$ is a constant. The parameters determined for α, n and Q_a for the SnAgCu alloys are given in Table 2.

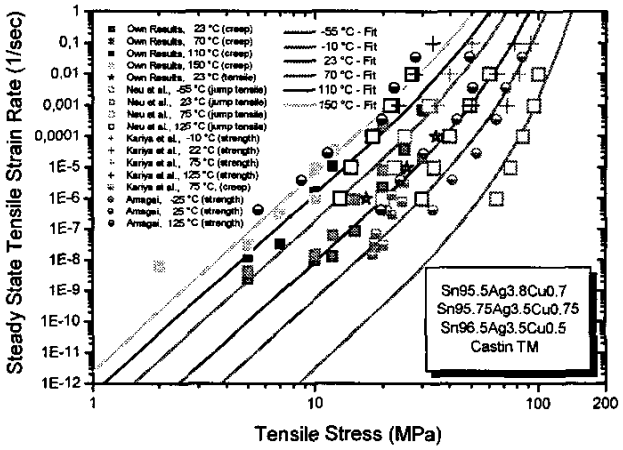

Figure 1: Curve-fitting of SnAgCu creep data to hyperbolic sine model (equation (2)), based on 108 data points from own measurements and literature.

Table 2: Deformation constants of the steady-state creep for SnAgCu-alloys, based on 108 data points from own measurements and literature (equation (2))

Sn95.5Ag3.8Cu0.7	$C_{III,IV}$	277984 s^{-1}
Sn95.75Ag3.5Cu0.75	α	0.02447 MPa^{-1}
Sn96.5Ag3.5Cu0.5	n	6.41
Castin™	Q_a	0.56 eV

Primary (Transient) Creep

Steady-state creep is not observed immediately when stress is applied (Figure 2). Transient (or primary) creep occurs before attaining steady state. For normal decelerating transient creep, the strain rate starts high and decreases to the steady state value. The creep composed of a primary and secondary part at constant stress and temperature can be described by the equation

$$\varepsilon_{cr} = \varepsilon_p^{sat}\left\{1 - \exp\left[-K\left(\frac{d\varepsilon_S}{dt}\right)^n\right]\right\} + \frac{d\varepsilon_S}{dt}t, \qquad (3)$$

where ε_p^{sat}, K and n are constants [4]. The saturated transient creep strain can be obtained by extrapolating the steady-state creep line back to the starting point.

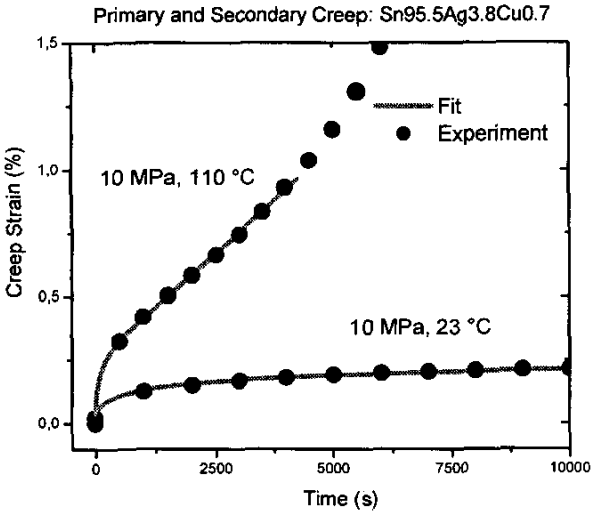

Figure 2: Creep of Sn95.5Ag3.8Cu0.7 composed of a primary and secondary part at constant stress and temperature, experimental curves and fitted by equation (3)

Taking the time-derivative of both sides of equation (3) yields

$$\frac{\varepsilon_{cr}}{dt} = n \; K \; \varepsilon_p^{sat} \left(\frac{d\varepsilon_s}{dt}\right)^n (t)^{n-1} \exp\left[-K \left(\frac{d\varepsilon_s}{dt}\right)^n\right] + \frac{d\varepsilon_s}{dt}, \quad (4)$$

where $\frac{\varepsilon_{cr}}{dt}$ is the total creep rate and $\frac{d\varepsilon_s}{dt}$ is the steady-state creep rate. For small times t, the instantaneous creep rate is greater than the steady-state creep rate (singular at t=0), and after a long time, the instantaneous rate approaches zero, and the total creep strain rate is equal to the steady-state rate.

Table 3: Deformation constants of the primary (transient) creep for Sn59Pb40Ag1 and Sn95.5Ag3.8Cu0.7, based on own measurements (equation (4))

	ε_p^{sat} (%)	K (s^{-1})	n
Sn59Pb40Ag1	0.4735	145	0.66
Sn95.5Ag3.8Cu0.7	0.4778	69	0.55

The coefficients of equation (4) were fitted to measuring results. However, only few measuring data was available. Table 3 shows the results achieved so far, slightly different for both the solder compositions. It should be mentioned, that a simplified form of equation (4), which was given by Darveaux et al. [5], was not capable of fitting the stress strain response for both solders in a reasonable way.

Young's Modulus, Coefficient of Thermal Expansion and Poisson's Ratio of the Used Solders

The temperature-dependent Young's modulus (E), the coefficient of thermal expansion (CTE) and Poisson's ratio (v) of the used solder materials are also entered as material properties in the strain-stress analysis of the investigated microelectronic packages.

Typical expansion coefficients for the different solders are shown in Table 4. The CTE value of the examined lead-free solder SnAgCu is smaller than that of SnPbAg. On the other hand, the Young's modulus of the lead-free alloy SnAgCu seems to be substantially higher than that of eutectic SnPbAg.

Another elastic property required in strain-stress analysis is Poisson's ratio. For both solder compositions a value of 0.36 was used in the FE-analyses, which were performed by use of the ABAQUS [6] software package.

Table 4: Young's modulus, Poisson's ratio and Coefficient of Thermal Expansion depending on temperature

	Young's Modulus [MPa]	Poisson's ratio	CTE (1/K)
Sn-Pb-Ag	36,000 at 210 K 21,000 at 398 K	0.36	$24.0\ 10^{-6}$
Sn-Ag-Cu	48,500 at 218 K 33,000 at 483 K	0.36	$20.0\ 10^{-6}$

Constitutive Relations of Other Materials

Besides solder, a package-PCB assembly also includes metals such as Ni-UBM, Cu-traces and metallizations, polymeric materials like epoxy mold compounds, die attach adhesives, solder masks and underfills, as well as FR-4 and BT used as interposer or substrates and the silicon die. Most of these materials have temperature dependent behaviors.

The behaviors of nickel and copper are both considered elastic-plastic. The polymeric underfills, solder mask epoxy mold compounds and die attach adhesives were treated as viscoelastic materials. FR-4 and BT interposers and substrates consist of layers of epoxy-glass laminate alternating with thin sheets of copper, and are assumed to be orthotropic. For these analyses, only the overall behavior of the interposer and substrate was of interest. Therefore, they were modeled as homogeneous materials. The anisotropic thermal expansion of the organic FR-4 and BT interposer and substrate as well as its elastic anisotropy are both accounted for in the analyses. The silicon die is treated as a linearly elastic body.

Fatigue Life Models

A quantitative comparison of the thermal fatigue lives of lead-free solder joints and lead-containing joints was made, assuming a similar low cycle fatigue behavior of the two solder materials. An empirical model has been used for a long time [7], which assesses the amplitudes of the accumulated creep strain ε_{cr}^{acc} along the damage path for estimation of

mean cycles to failure N_f by simple application of a Coffin-Manson type relation:

$$N_f = \Theta_1(\varepsilon_{cr}^{acc})^{-c1}. \quad (5)$$

ε_{cr}^{acc} is the actual minimum (or average) over the path of local maximum equivalent creep strain.

Besides creep strain criteria, also creep strain energy-based methods have been applied to determine the fatigue of solder joints. The equation is to be read in terms of viscoplastic energy density:

$$N_f = \Theta_2(\Delta W_{cr}^{acc})^{-c2}, \quad (6)$$

where ΔW_{cr}^{acc} is the actual minimum (or average) over the path of local maximum of viscoplastic strain energy density, dissipated per cycle.

That means, an approach similar to that for the equivalent creep strain was chosen with regard to the distribution pattern of the creep energy density: The local minimum (or average) of a band of maximum creep energy density crossing the volume of the solder joints is assumed to determine the critical cycle number. The viscoplastic strain energy density is defined as the summation of the scalar product of stress and inelastic strain increment tensors.

Investigated Assemblies and Thermal Cycling Conditions

For these models to be more reliable, the empirical correlation of life data should hold over a minimum of three orders of magnitude on the horizontal (experimentally determined characteristic life) and vertical axis (damage parameters, e.g. creep strains accumulated in one thermal cycle or the average viscoplastic strain energy dissipated per cycle). To fulfill these requirements three different assemblies were chosen and tested under different thermal cycling conditions.

Flip Chip on Organic Board Without Underfill

To analyze the low thermal cycle range of some hundred cycles, a flip chip on board assembly without underfill was investigated. For the low cycle range, a silicon chip, having two peripheral bump rows with a pitch of 450 µm, was used as the first test vehicle. The die size was 6.7 x 6.7 mm and had electroless NiP as under bump metallization (UBM). The die was flip-chip bonded to a 0.9 mm organic substrate made of FR-4 and solder mask. The metal finish of the substrate was Cu/NiAu. Three air-to-air thermal cycling conditions were chosen for the evaluation, -50 °C to 20 °C, 0 °C to 70 °C and 50 °C to 120 °C, all at a frequency of 30 min per cycle with dwell times of 10 min and ramp times of 5 min.

Flip Chip on Organic Board With Underfill

To extend the thermal cycle range to numbers of about 1000 and larger cycles, a flip chip on organic board with underfill was chosen simultaneously. However, because of failure mode mixing of underfill delamination and solder fatigue, the testing data should be treated with care [8]. In our experiments, cross sectioning has revealed solder fatigue as the dominating failure mode.

As test chips, 10 x 10 mm^2 sized silicon dice with a 300 µm pitch were used. The aluminum pads were coated with electroless nickel UBM. The chips were placed onto the 1.0 mm high Tg FR-4 substrate with Cu/NiAu as metal finish. Hysol FP 4511 underfill material was selected for the assemblies. The underfill was applied and cured according to its specific requirements.

For the reliability investigations and the comparison with the simulation results, two thermal cycling profiles were selected for a total cycle time of 30 min (10 min dwells, triple zone chamber cycling), 125 °C ... –55 °C and 150 °C ... –55 °C in order to allow direct comparison.

Plastic Ball Grid Arrays (PBGA 256 and 272)

To reach the range of 5000 to 10000 thermal cycles, a family of wire-bonded plastic BGAs with optimized design for maximum board-level reliability were chosen. PBGAs with pin counts of 256 and 272 and with ball pitches of 1.27 mm were analyzed, see also [9],[10]. The PBGA 272 is a four row perimeter PBGA with thermal balls. This package includes a die in size of 10 x 10 x 0.35 mm^3, BT-substrate thickness of 0.56 mm and solder mask defined pads. The PBGA is mounted onto a 1.57 mm high Tg FR-4 board. For the PBGA 256 the same geometry was used, but without thermal balls underneath the die. To establish reliable lifetime models, some experimental reliability data from the literature [11] were also included in the evaluation. Reliability data from the commonly used –40 °C to 125 °C thermal cycling condition as well a more severe condition of –40 °C to 150 °C were analyzed to include the PBGAs reliability in the lifetime prediction models.

Experimental Reliability Results

The small amount of data from literature shows that although the joint reliability can be increased by the use of SnAgCu or SnAg alloys, the degree of improvement is package dependent. The reliability improvement should be better for a more compliant package-board assembly (e.g. PBGA). For package types with high CTE mismatch to the board (e.g. LCCC assembled on FR-4), the solder joint reliability may decrease by using lead-free solders like SnAgCu or SnAg [12].

Furthermore, the comparison of different cycling conditions indicates different acceleration factors. For instance, a CBGA-625 package with SnAgCu solder joints performs worse in a severe test condition (with increasing peak temperature and increasing temperature interval of the thermal cycle) than in a more benign condition, [13], [14].
In the following, the experimental reliability results for different package assemblies are given.

If sufficient failures were recorded during temperature cycling, the cycles to failure for the flip-chip configurations without underfill were determined by a two-parameter Weibull analysis. The two parameters of this distribution are beta, which is the Weibull slope and eta, which is the Weibull characteristic life, or cycles to 63.2 % package failure, or the mean-time-to-failure at about 50 % failure.

For the flip-chip assemblies without underfill, Figures 3 and 4 show the lognormal failure probability plots of the tests

with the –50 °C to 20 °C and 50 °C to 120 °C temperature ranges and 30 min cycle times. Both ranges maintain the same temperature difference of 70 °C.

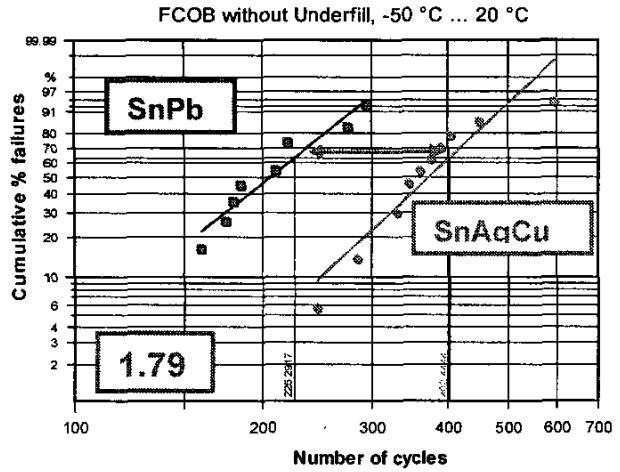

Figure 3. FCOB without underfill, solder joint reliability comparison of SnAgCu alloy with SnPb eutectic for –50 °C to 20 °C, ATC condition.

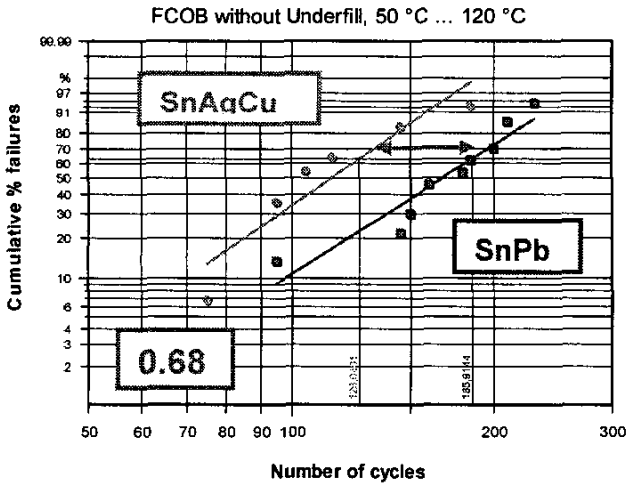

Figure 4. FCOB without underfill, solder joint reliability comparison of SnAgCu alloy with eutectic SnPb for 50 °C to 120 °C ATC condition.

The data for the lead-free alloy during –50 °C to 20 °C air-to-air thermal cycle (ATC) test demonstrate an approximately 1.8 fold longer fatigue life for the SnAgCu bumps than for the SnPb bumps. Under 50 °C to 120 °C cycling test conditions, it is clear that the relative fatigue performance of both alloys is fundamentally different from that for the –50 °C to 20 °C range. The SnAgCu flip chip modules have only 2/3 of the fatigue life of the SnPb bumped modules.

The summary of temperature cycle data on these stiff assemblies, given in Figure 5, indicates that the acceleration factors depend on accelerated test conditions and the solder alloys. The data clearly shows that the SnAgCu alloy considered here has resulted in higher acceleration factors compared to the SnPb alloy when comparing the different temperature cycling conditions. Obviously it is possible that the treated stiff package with SnAgCu alloy joints performing worse in a severe test condition may actually perform better in a more benign condition.

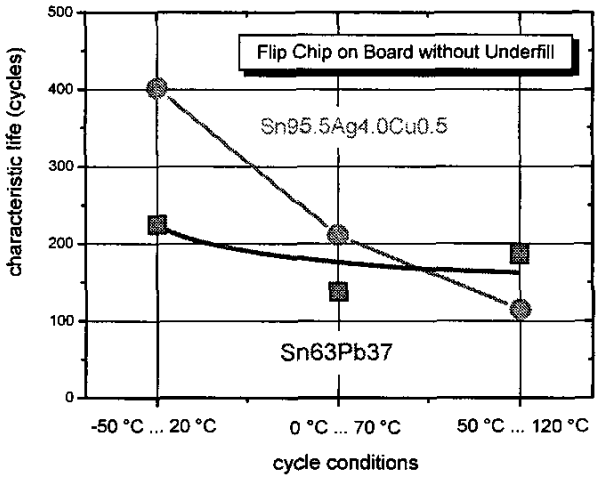

Figure 5. Solder joint reliability comparison of SnAgCu alloy with SnPb eutectic for FCOB, without underfill and under different temperature cycling conditions.

The impact of the SnAgCu solder compositions on the reliability of flip-chip assemblies with underfill was studied experimentally and compared to SnPb solder. The assemblies were temperature cycled at two different temperature ranges: –55 °C to 125 °C and –55 °C to 150 °C. Again, the cycles to failure for these flip-chip configurations were determined by a two-parameter Weibull analysis in those cases when sufficient failures were recorded during temperature cycling.

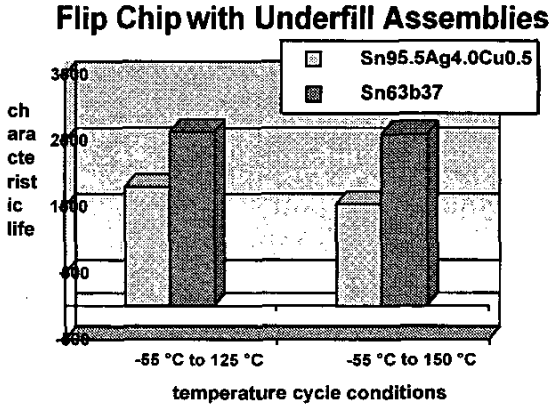

Figure 6. Characteristic life of FC with underfill assemblies for SnAgCu and SnPb solder, two temperature cycling conditions: 125 °C to -55 °C and 150 °C to -55 °C

Table 5: Thermal cycling characteristic life for PBGA-organic board assemblies with Sn-Ag-Cu and SnPb solder joints

PBGA-type (No. of I/O, body size) Thermal cycling condition source	Caracteristic Life	
	Sn-Ag-Cu	SnPb
PBGA-256 (27 x 27 mm^2) -40 °C to 125 °C, 60 min A. Syed	8083	3798
PBGA-272 (27 x 27 mm^2) -40 °C to 125 °C, 60 min A. Mawer et al.		5560
PBGA-272 (27 x 27 mm^2) -40 °C to 150 °C, 44 min own measurements		2814
PBGA-316 (35 x 35 mm^2) -40 °C to 125 °C, 60 min Shi-Wei Ricky Lee et al.	3664 - 4187	2603
PBGA-313, (27 x 27 mm^2) -40 °C to 125 °C, 60 min Shi-Wei Ricky Lee et al.	4465 - 4917	2826

Figure 6 shows a solder joint reliability comparison for the SnAgCu alloy with SnPb eutectic for both cycling conditions. Under both ATC test conditions, the critical cycle numbers are slightly reduced for the SnAgCu solder alloy when compared to the SnPb solder alloy. Furthermore, only a small difference for both solder compositions was detected for the two temperature cycling conditions: 125 °C to -55 °C and 150 °C to -55 °C.

To reach much higher numbers of temperature cycles, PBGAs were considered for the evaluation of lifetime models in the following analysis. The board reliability of PBGAs on board assemblies is much larger than for the assemblies considered above. Table 5 shows that for packages with low CTE mismatch with the board, e.g. PBGAs mounted on FR-4, the solder joint reliability may actually increase by using SnAgCu alloys. In other words, the reliability improvement is better for SnAgCu alloys used in a more compliant package-board assembly with lower solder straining, like PBGA on board.

Figure 7 shows the correlation of fatigue life data from different accelerated tests on different package types with SnPb(Ag) and SnAgCu interconnects versus the determined accumulated creep strains by FEA in the solder interconnects. If equation (5) holds, the curve fitting has to be a straight line in a log-log plot. It can be observed from the diagram that this behavior is approximately true. The life prediction models for SnPb(Ag) and SnAgCu solder interconnects based on the best-fit line going through the data of 14 experiments.
The results suggest that SnAgCu thermo-mechanical failure data may correlate to accumulated creep strains as in the case of eutectic SnPb(Ag) soldered assemblies. In Figure 7, the slope of the best-fit line through the SnPb(Ag) data is −1.80 and for the SnAgCu data about −1.3. Furthermore, a crossover point between the two alloys is indicated at approximately 600 – 800 cycles.

These findings suggest that for the same strain level at higher strains, SnAgCu performs better, whereas for the same strain level at lower strains, SnPb(Ag) performs better.

A similar trend was found for the correlation of the thermo-mechanical failure data to the calculated viscoplastic strain energy density, as shown in Figure 8. In that case, a crossover point between the two alloys is indicated, at approximately 6000 – 8000 cycles. But these findings also suggest that for the same strain level at higher energy densities SnAgCu performs better, whereas for the same energy density, SnPb(Ag) performs better. The determined slope of the best-fit line through the SnPb(Ag) data is −1.20 and for the SnAgCu data about −1.0.

Summary

Based on materials testing as well as data given in the literature, the constitutive behavior of Sn95.5Ag3.8Cu0.7 solder is described by a creep law and compared to the creep behavior of Sn59Pb40Ag1 solder. The creep rates given for both solders contain a primary and a secondary part. However, investigations on the primary creep description are still ongoing. Improved predicting capabilities are expected to be derived from inclusion of a primary part, especially for varying cycling conditions, e.g. air-to-air, liquid-to-liquid, or field cycle conditions. These expectations have been confirmed by the first simulation results.

Combined experimental and theoretical investigations on electronic assemblies were performed to describe the fatigue behavior of SnAgCu solder and its mathematical prediction, based on empirical power-law relationships. It is shown that the experimental data can be fitted reasonably well by such a relationship for both equivalent creep strain and dissipated creep strain energy density. When the SnAgCu data is compared to SnPb solder, similar coefficients are observed in the empirical fatigue relations. However, the results suggest that for the same strain level at higher strains, SnAgCu performs better, whereas for the same strain level at lower strains, SnPb(Ag) performs better. These differences as well as the different creep behaviors of the two solders cause the experimentally observed trend of an improved fatigue life of SnPb solder joints for relatively stiff components and high thermal mismatch induced loads, compared to a better performance of SnAgCu solder for relatively compliant structures and low thermal mismatch induced loads.

Acknowledgments

The authors would like to express their thanks to H. Walter, IZM Berlin, for his materials testing work. The assistance of Mr. R. Döring, CWM GmbH Chemnitz, in performing the FE-modeling, was gratefully appreciated.

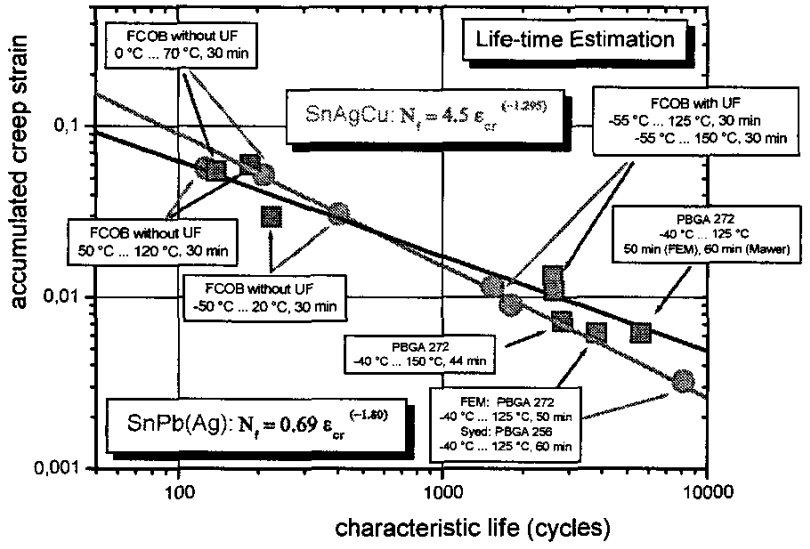

Figure 7: SnPb(Ag) and SnAgCu fatigue life versus accumulated creep strain during one thermal cycle

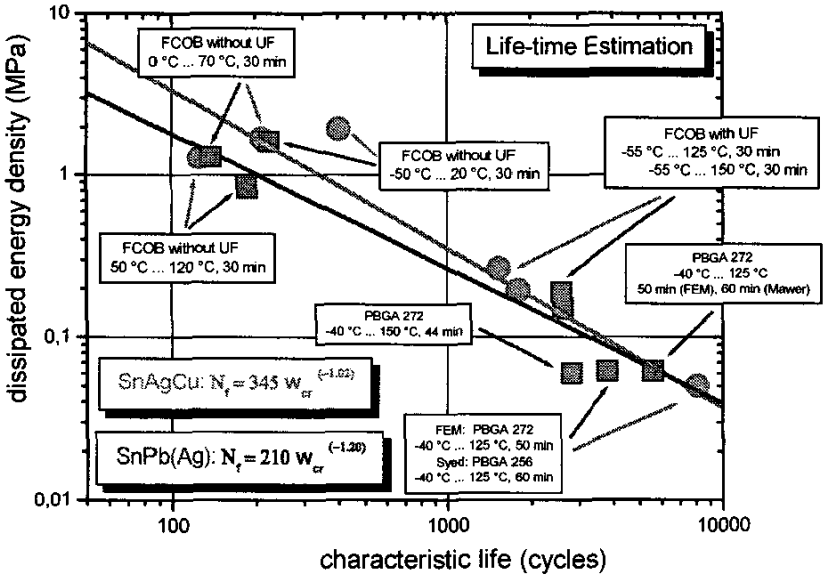

Figure 8. SnPb(Ag) and SnAgCu fatigue life versus dissipated energy density during one thermal cycle

References

[1] Grivas, D., Murty, K.L., Morris, J. W. Jr., "Deformation of Pb-Sn Eutectic Alloys at Relatively High Strain Rates", *Acta Metallurgica*, 27 (1979), pp. 731-737

[2] Hacke, P.L.; Sprecher, A.F., Conrad, H., "Thermo-mechnical Fatigue of 63Sn-37Pb Solder Joints"
in Lau, J.H.: Thermal Stress and Strain in Microelectronics Packaging, Van Nostrand Reinhold, 1993, pp.467-499

[3] Schubert, A., Dudek, R., Walter, H., Jung, E., Gollhardt, A., Michel, B., Reichl, H., "Reliability Assessment of Flip-Chip Assemblies with Lead-free Solder Joints", *Proc. 52nd Electronic Components & Technology Conf. (ECTC)*, San Diego, USA, May 28-31, 2002, Proc. pp. 1246-1255.

[4] Mayuzumi, M., Onchi, T., "Creep Deformation and Rupture Properties of Unirradiated Zircaloy-4 Nuclear Fuel Cladding Tube at Temperatures of 727 to 857 K", *Journal of Nuclear Materials*, 175 (1990), pp. 135-142.

[5] Darveaux, R., Banjerji, K., Mawer, A., Dody, G.; "Reliability of Plastic Ball Grid Array Assembly"
in H. Lau (ed.): Ball Grid Array Technology, McGraw-Hill, New York, 1995, pp. 379-442

[6] ABAQUS *User Manuals* (V. 6.1), Hibbitt, Karlsson and Sorensen, Inc., Providence, RI, 2000

[7] Dudek, R.; Nylen, M., Schubert, A., Michel, B., Reichl, H., "An Efficient Approach to Predict Solder Fatigue Life and its Application to SM- and Area Array Components,"
Proc. of ECTC 47, San Jose, May 1997, pp. 462-471.

[8] Schubert, A.; Dudek, R.; Leutenbauer, R.; Döring, R.; Kloeser, J.; Oppermann, H.; Michel, B.; Reichl, H.; Baldwin, D.; Qu, J.; Sitaraman, S.; Swaminathan, M.; Wong, C.P.; Tummala, R., "Do Chip Size Limits Exist for DCA?", *IEEE Transactions on Electronics Packaging Manufacturing*, Vol. 22, No. 4, Oct. 1999, pp. 1-8.

[9] Dudek, R., Döring, R., Michel, B., "Reliability Prediction of Area Array Solder Joints," *Proc. Internat. Conference EuroSimE 2001*, Paris, France, April 2001, pp. 215-222.

[10] Schubert, A., Dudek, R., Döring, R., Walter, H., Auerswald, E., Gollhardt, A., Schuch, B., Sitzmann, H., Michel, B., "Lead-free Solder Interconnects: Characterization, Testing and Reliability", *Proc. 3rd Int. Conf. on Benefiting from Thermal and Mechanical Simulation in (Micro)-Electronics (€SIME)*, Paris, France, April 15-17, 2002, Proc. pp. 62-72.

[11] Mawer, A. J., Nick Vo, Johnson, Z., Lindsay, W., "Board-Level Characterization of 1.0 and 1.27 mm Pitch PBGA for Automotive Under-Hood Applications", *Proceedings 49th Electronic Components & Technology Conference*, 1999.

[12] Syed, A., "Reliability and Au Embrittlement of Lead Free Solders for BGA Applications", *Proc. Intern. Symposium and Exhibition on Advanced Packaging Materials*, Braselton, Georgia, USA, March 11-14, 2001, pp. 143-147.

[13] Syed, A., "Reliability of Lead-free Solder Connections for Area-Array Packages," *Proc. IPC SMEMA Council*, APEX, LF2-7, pp. 1-9.

[14] Bartelo, J., Cain, S.R., Caletka, D., Darbha, K., Gosselin, T., Henderson, XD.W., King, D., Knadle, K., Sarkhel, A., Thiel, G., Woychiik, C., Shih, D. Y., Kang, S., Puttlitz, K., Woods, J.., "Thermomechanical Fatigue Behavior of Lead-free Solders," *Proc. IPC SMEMA Council*, APEX 2001, San Diego, CA, Jan. 2001, LF2-2, pp. 1-11.